



# Polymethylhydrosiloxane-modified gas-diffusion cathode for more efficient and durable H<sub>2</sub>O<sub>2</sub> electrosynthesis in the context of water treatment

Pan Xia<sup>a</sup>, Lele Zhao<sup>b</sup>, Xi Chen<sup>a</sup>, Zhihong Ye<sup>a,\*</sup>, Zhihong Zheng<sup>a</sup>, Qiang He<sup>a</sup>, Ignasi Sirés<sup>b,\*</sup>

<sup>a</sup> Key Laboratory of Eco-environments in Three Gorges Reservoir Region, Ministry of Education, College of Environment and Ecology, Chongqing University, Chongqing 400045, China

<sup>b</sup> Laboratori d'Electroquímica dels Materials i del Medi Ambient, Departament de Ciència de Materials i Química Física, Secció de Química Física, Facultat de Química, Universitat de Barcelona, Martí i Franquès 1–11, 08028 Barcelona, Spain

## ARTICLE INFO

### Keywords:

Electro-Fenton process  
Gas-diffusion electrode  
Electrocatalytic hydrogen peroxide synthesis  
Oxygen reduction reaction  
Siloxane

## ABSTRACT

On-site H<sub>2</sub>O<sub>2</sub> electrosynthesis via two-electron oxygen reduction reaction (ORR) is attracting great interest for water treatment. The use of carbon black-based gas-diffusion electrodes (GDEs) is especially appealing, but their activity, selectivity and long-term stability must be improved. Here, a facile GDEs modification strategy using trace polymethylhydrosiloxane (PMHS) allowed reaching an outstanding H<sub>2</sub>O<sub>2</sub> production, outperforming the conventional polytetrafluoroethylene (PTFE)-GDE (1874.8 vs 1087.4 mg L<sup>-1</sup> at 360 min). The superhydrophobicity conferred by PMHS endowed the catalytic layer with high faradaic efficiencies (76.2%–89.7%) during long-term operation for 60 h. The electrochemical tests confirmed the high activity and selectivity of the PMHS-modified GDE. Moreover, the efficient degradation of several micropollutants by the electro-Fenton process demonstrated the great potential of the new GDE. An in-depth understanding of the roles of PMHS functional groups is provided from DFT calculations: the –CH<sub>3</sub> groups contribute to form a superhydrophobic interface, whereas Si-H and as-formed Si-O-C sites modulate the coordination environment of active carbon centers.

## 1. Introduction

Hydrogen peroxide (H<sub>2</sub>O<sub>2</sub>), an eco-friendly and versatile oxidant with only H<sub>2</sub>O and O<sub>2</sub> as by-products, has been intensively employed for environmental remediation, as well as in medical disinfection or industrial bleaching and synthesis [1–3]. Nonetheless, critical risks associated with transportation, storage and manipulation of H<sub>2</sub>O<sub>2</sub> pose extraordinary technological and economic challenges that limit its application [4,5]. In addition, the anthraquinone process for industrialized production of H<sub>2</sub>O<sub>2</sub> has serious limitations, such as high-energy consumption and substantial waste generation [6]. In this context, the in-situ electrosynthesis of H<sub>2</sub>O<sub>2</sub> via the two-electron oxygen reduction (2e<sup>-</sup> ORR) opens up a new avenue to the H<sub>2</sub>O<sub>2</sub> market [7,8].

The electro-Fenton process (EF), one of the most popular advanced technologies for wastewater treatment, combines the merits of both Fenton's reaction and 2e<sup>-</sup> ORR [9,10]. Its successful implementation at large scale highly relies on the cathodic H<sub>2</sub>O<sub>2</sub> yield. For this, molecular oxygen must be efficiently reduced to H<sub>2</sub>O<sub>2</sub> via the so-called 2e<sup>-</sup> pathway (Reaction (1)), which occurs upon co-existence of a triple phase

(i.e., O<sub>2</sub> gas and hydrated proton at the catalytic surface site) during the electron supply. Therefore, the gas-liquid-solid balance at the three-phase boundary is of paramount importance for efficient H<sub>2</sub>O<sub>2</sub> production [8,11]. Carbonaceous materials are usually preferred as the electrocatalyst in EF due to their favorable activity and H<sub>2</sub>O<sub>2</sub> selectivity, low cost, and moderate durability at low-medium current [12–14].

In recent years, most efforts to improve the cathodic H<sub>2</sub>O<sub>2</sub> yield have focused on the enhancement of O<sub>2</sub> mass transport, electron transfer, and H<sub>2</sub>O<sub>2</sub> selectivity [15,16]. For this purpose, the gas-diffusion electrode (GDE) architecture is widely employed [12,17,18]. The utilization of a GDE as the cathode minimizes the barrier to O<sub>2</sub> permeation through the cavities to the catalytic sites, overcoming the low solubility (8 mg L<sup>-1</sup>) and poor diffusion rate of O<sub>2</sub> that are inherent to immersed cathodes [3]. However, even with GDEs, the production of H<sub>2</sub>O<sub>2</sub> cannot reach its maximum during long-term operation [19], which is partly caused by flooding due to insufficient hydrophobicity, leading to the inactivation of the catalytic layer [19–21]. On the other hand, due to the competing scaling relationship between the 2e<sup>-</sup> ORR (Reaction (1)) to form H<sub>2</sub>O<sub>2</sub> and the 4e<sup>-</sup> ORR (Reaction (2)) to generate H<sub>2</sub>O, the strategies aimed at

\* Corresponding authors.

E-mail addresses: [yezhihong@cqu.edu.cn](mailto:yezhihong@cqu.edu.cn) (Z. Ye), [i.sires@ub.edu](mailto:i.sires@ub.edu) (I. Sirés).

<https://doi.org/10.1016/j.apcatb.2023.123467>

Received 22 August 2023; Received in revised form 9 October 2023; Accepted 2 November 2023

Available online 4 November 2023

0926-3373/© 2023 The Author(s). Published by Elsevier B.V. This is an open access article under the CC BY-NC-ND license (<http://creativecommons.org/licenses/by-nc-nd/4.0/>).

improving the former frequently enhance the  $4e^-$  pathway as well [22, 23].



The construction of stable superhydrophobic three-phase boundaries in GDEs has been proven a successful approach to increase the  $O_2$  utilization efficiency and decrease the cathode flooding. In 2015, Yu and co-workers employed polytetrafluoroethylene (PTFE) as hydrophobizing material to fabricate a water-proof GDE, obtaining a 10.7-fold increase in  $H_2O_2$  concentration at 60 min under an optimal PTFE/carbon black (CB) mass ratio of 5 [24]. In such cathode, the hydrophobic sites confine the  $O_2$  bubbles, thereby feeding the hydrophilic sites where the  $2e^-$  ORR occurs in the presence of hydrated protons. Significant efforts have been further made to regulate the hydrophilicity/hydrophobicity ratio. Zhang et al. claimed that a CB-to-PTFE ratio of 5:3 yielded the highest  $H_2O_2$  production efficiency [25], whereas He et al. reported that the yield of  $H_2O_2$  varied insignificantly when the mass ratio of graphite to PTFE was decreased [26]. However, although the introduction of PTFE seems to be a facile and effective way to enhance the  $O_2$  supply and avoid excessive water transport into the pores, it may block the catalytic sites.

The development of selective electrocatalysts to ensure both, the systematic control of the  $2e^-$  ORR route and the improvement of their catalytic activity, is another effective strategy to synthesize  $H_2O_2$ . The  $2e^-$  ORR associative pathway proceeds through two main steps, namely  $O_2$  activation (Reaction (3)) and further reduction of the  $*OOH$  intermediate (Reaction (4)). In contrast, the competitive  $4e^-$  ORR pathway involves three reaction intermediates ( $*OOH$ ,  $*O$ , and  $*OH$ ) [27]. Therefore,  $H_2O_2$  can be selectively formed if one can ensure that  $*OOH$  is the only intermediate [28], and it is neither too strongly nor too weakly bound to the catalyst surface, aiming at preventing the O–O bond dissociation, as has been determined via density functional theory (DFT) calculations [29]. So far, a wide range of electrocatalysts has been designed to fabricate GDEs with enhanced  $2e^-$  ORR activity/selectivity, including modified carbon materials, non-noble metal-nitrogen moieties, molecular complexes, and single-atom catalysts [3,8,18]. These electrocatalysts may play one or several roles [30–33]. Nonetheless, these catalyst layers usually own weak bonds and low tolerance to acidic conditions. As a result, they can be gradually dissolved, especially during long electrolytic trials, causing severe electrode deactivation.



Recently, silicon derivatives have been proposed as surface modifiers to improve water proof and  $O_2$  transport for  $H_2O_2$  production [20]. Among these compounds, polysiloxanes have demonstrated their utility in fabricating  $O_2$ -selective membranes for Li-air batteries with low water transport [34]. In particular, polymethylhydrosiloxane (PMHS,  $-(CH_3(H)Si-O)-$ ), a non-toxic and easy-to-handle hydride source, has been widely employed as hydrophobic modifier as well as catalytic center in chemical synthesis and membrane separation, since it can be chemically attached to the surface of substrates while retaining the functional groups for further catalytic reactions [35,36]. PMHS contains a large number of  $-CH_3$  and  $-Si-H$  groups. The former own low surface energy, becoming optimum to construct highly hydrophobic interfaces [37–39]. For instance, Liu et al. prepared a filter paper/PMHS hybrid with a surface water contact angle ranging from  $9.0^\circ$  to  $131.8^\circ$  by regulating the PMHS dosage [40]. On the other hand, the  $-Si-H$  groups may serve as chemical links to react with the unsaturated  $C=C$  or  $HO-C$  bonds of substrates, resulting in the formation of  $Si-O-C$  moieties. Wójcik-Bania et al. reported the in-situ reduction of  $Pt^{4+}$  from  $PtCl_4$  solution to  $Pt^0$  by the  $Si-H$  moieties of the siloxane backbone of PMHS under an inert atmosphere [41]. Moreover, it has been proven that

Si-doped graphene material is a promising  $4e^-$  ORR catalyst due to the presence of abundant Si-O sites, which favors the adsorption and dissociation of  $O_2$  [42,43].

Only very recently, the potential combination of polysiloxanes and hydrophobic perfluorinated polymers has been suggested as a promising strategy for the fabrication of gas-diffusion layers, although it has been not explored in the context of the  $2e^-$  ORR [44]. Inspiringly, the present study focuses on the utilization of trace PMHS to modify PTFE-GDEs, for the first time, aiming at synchronously enhancing the  $O_2$  permeability and  $H_2O_2$  selectivity for ORR. The  $-CH_3$  groups of PMHS are expected to confer stable superhydrophobicity to the catalytic interface, whereas the Si-H bonds, as well as the as-formed Si-O-C moieties, might serve as new active sites to enhance the  $2e^-$  ORR.

## 2. Materials and methods

### 2.1. Chemicals

2,4 Dichlorophenol (2,4-DCP) and naproxen (NPX) were purchased from Aladdin Biological Technology Co., Ltd. (Shanghai, China). Analytical grade  $Na_2SO_4$ ,  $H_2SO_4$  (95% solution), NaOH pellets, and  $FeSO_4 \cdot 7 H_2O$  were supplied by Chengdu Kelong Chemical Co., Ltd. (Chengdu, China). Bisphenol A (BPA), ciprofloxacin (CIP), amoxicillin (AMX), diclofenac sodium (DCF), Rhodamine B (RhB), Methyl Orange (MO), poly(dimethylsiloxane)etherimide (PDMS-NH<sub>2</sub>), 1,3-bis-(dichloromethyl)-1,1,3,3-tetramethyldisiloxane (PDMS-Cl) and polymethylhydrosiloxane (PDMS-H or PMHS) were acquired from Macklin Technology Co., Ltd. (Shanghai, China). Nafion (5 wt% suspension in lower aliphatic alcohol) was purchased from Sigma-Aldrich (Shanghai, China). PTFE emulsion (60 wt%) was purchased from Hesen Co., Ltd. (Henan, China). 1,10-Phenanthroline monohydrate, L(+)-ascorbic acid and  $TiOSO_4$  were used for colorimetric analyses. Solvents and other reagents were supplied by Merck and Chengdu Kelong Chemical Co., Ltd. (Chengdu, China). Unless otherwise specified, all chemicals were of analytical grade and used as received, and all solutions were prepared with deionized water (resistivity higher than  $18.2 M\Omega \cdot cm$ , Millipore Milli-Q system).

### 2.2. Cathode preparation

The gas-diffusion electrode consisted of a mixture of carbon black and PTFE, with or without PMHS modification, acting as catalytic and gas-diffusion layers that served to coat a carbon cloth substrate (Fig. 1a). To prepare the GDE, commercial cloth with a geometric area of  $9 cm^2$  was ultrasonically cleaned in deionized water and ethanol, each for 30 min, and then dried at  $80^\circ C$  for 12 h. Then, 200 mg carbon black, 0.685 mL PTFE (60 wt% emulsion) and a certain amount of PMHS were uniformly dispersed in 10 mL ethanol using an ultrasonic bath for 30 min, followed by heating at  $80^\circ C$  until the mixture turned into a paste. The ointment was coated onto the pretreated carbon cloth substrate, followed by pressing at 5 MPa. The resulting electrode was dried and calcined at  $350^\circ C$  for 120 min to obtain the PTFE/PMHS-GDE. For comparison, the same manufacturing procedure was carried out in the absence of PMHS, giving rise to the conventional PTFE-GDE.

### 2.3. Performance evaluation and analytical methods

The electrolytic trials were carried out under continuous stirring in a single-compartment glass cell containing 160 mL of solution equipped with an  $IrO_2$ -based dimensionally stable anode (DSA) plate ( $3 cm^2$ ) from NMT Electrodes and one of the as-prepared GDEs as the cathode. The interelectrode gap was 1.0 cm, and the GDE was fed with air at  $1 L min^{-1}$  for permanent  $H_2O_2$  electrogeneration. The trials were carried out galvanostatically by supplying a constant current from a high-stability DC voltage controller (IT6302 from ITECH, China). In EF trials, a salt was employed as  $Fe^{2+}$  source that served as Fenton's catalyst.

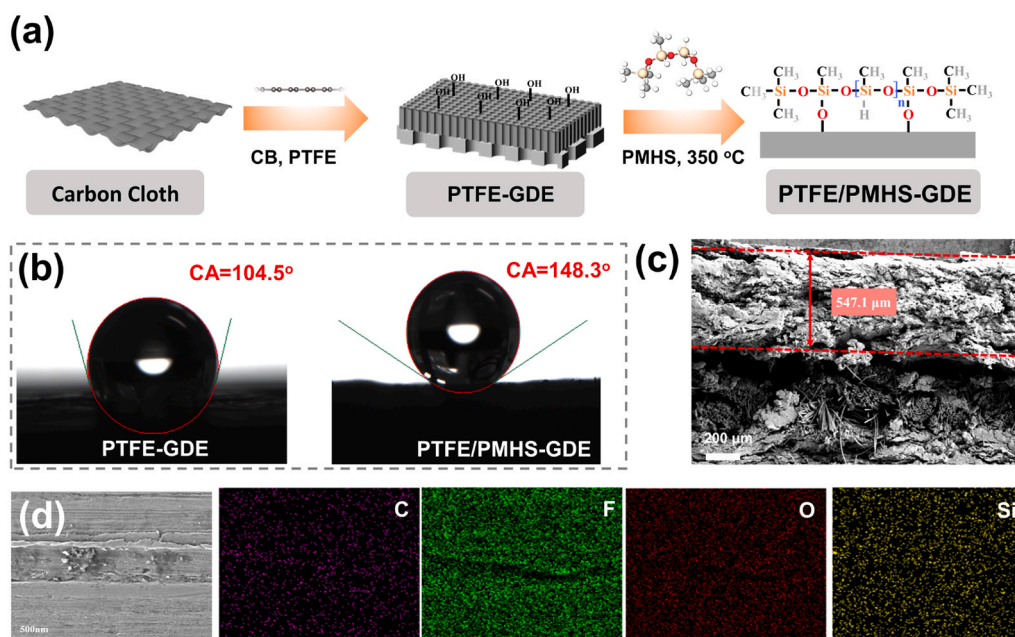


**Fig. 1.** (a) Schematic illustration of PTFE/PMHS-GDE fabrication. (b) Contact angle of conventional PTFE-GDE and novel PTFE/PMHS-GDE. SEM images of (c) cross-section and (d) surface of PTFE/PMHS-GDE, with the corresponding surface EDS elemental mapping.

Samples were collected at different time intervals, being immediately mixed with NaOH to quench the reaction and then filtered with 0.2  $\mu\text{m}$  PTFE syringe filters. The solution pH was determined using a PHS-3 C pH-meter. The accumulated  $\text{H}_2\text{O}_2$  concentration was measured colorimetrically, by mixing the collected sample with an acidic Ti(IV) solution and then setting the UV/Vis spectrophotometer (UNIC, UV2365, China) at  $\lambda = 408$  nm. The Faradaic efficiency (FE) for  $\text{H}_2\text{O}_2$  generation was calculated from Eq. (5) [30].

$$\text{FE}(\text{in}\%) = \frac{2C_{\text{H}_2\text{O}_2} FV}{\int_0^t I dt} \times 100 \quad (5)$$

where  $F$  is the Faraday constant ( $\text{C mol}^{-1}$ ),  $C$  is the concentration of  $\text{H}_2\text{O}_2$  ( $\text{mol L}^{-1}$ ),  $V$  is the solution volume (L),  $I$  is the applied current (A), and  $t$  is the reaction time (s).

The concentration of micropollutants was determined on a reversed-phase high-performance liquid chromatograph (HPLC, SCION6000, China) equipped with a Chromcore C18 ( $5 \mu\text{m}$ ,  $4.6 \text{ mm} \times 250 \text{ mm}$ ) column and a photodiode array SC6000 detector. The mobile phase was a mixture of  $\text{CH}_3\text{OH}$  and 10 mM  $\text{KH}_2\text{PO}_4$  solution at pH 4.0 (80:20 (v/v)) that was eluted at  $1.0 \text{ mL min}^{-1}$ .

#### 2.4. Characterization and electrochemical tests

The morphology and elemental composition of the GDEs were analyzed by SEM-EDX, which was conducted on a ZEISS Gemini 300 SEM microscope coupled to a Smartedx detector operated in backscattering electron mode at an acceleration voltage of 15 kV. The chemical composition and state were determined by XPS on a Thermo Scientific K-alpha system with Al  $K\alpha$  radiation at a high voltage of 12 kV, calibrated internally using the C 1s ( $E_b = 284.80$  eV). The hydrophobicity of the GDEs was investigated by measuring the water contact angle on an interface tension meter (SDC-100S).

Cyclic voltammetry (CV), linear sweep voltammetry (LSV) and electrochemical impedance spectroscopy (EIS) were conducted on an electrochemical workstation (CHI 760E, Chenhua, Shanghai), equipped with a three-electrode cell that comprised a working electrode (glassy carbon, 3-mm disk), Ag/AgCl (saturated KCl) as reference electrode, and

a Pt sheet as counter electrode. The catalyst ink (CB-PTFE/PMHS) was prepared by dispersing carbon black (10 mg) in a solvent mixture consisting of 800  $\mu\text{L}$  of  $\text{H}_2\text{O}$  + 200  $\mu\text{L}$  of isopropanol + 50  $\mu\text{L}$  of Nafion (5 wt% suspension) + 50  $\mu\text{L}$  of PTFE (60 wt% suspension), and a certain amount of PMHS, followed by 30 min sonication. Subsequently, 10  $\mu\text{L}$  of catalyst ink were drop-casted onto a glassy carbon electrode, resulting in a catalyst loading of  $\sim 1.4 \text{ mg cm}^{-2}$ . For comparison, the CB-PTFE ink was prepared using the same procedure but in the absence of PMHS. LSV measurements were performed in  $\text{O}_2$ -saturated 0.05 M  $\text{Na}_2\text{SO}_4$  aqueous solution at room temperature at a scan rate of  $10 \text{ mV s}^{-1}$  within the potential range from 0.6 to  $-0.4$  V vs RHE. EIS analysis was made in the frequency domain from 0.01 Hz to 100 kHz at an alternating current signal amplitude of 5 mV. Cyclic voltammograms were obtained in  $\text{Fe}(\text{CN})_6^{4-} + \text{Fe}(\text{CN})_6^{3-}$  (each at 0.01 M) aqueous solution with a scan rate of  $10 \text{ mV s}^{-1}$ , within a range from  $-0.2$ – $1.4$  V vs RHE, and the electrochemical surface area (ECSA) was calculated from the Randles-Sevcik Eq. (6) [11].

$$I_p = 2.69 \times 10^5 ACD^{1/2}n^{3/2}\nu^{1/2} \quad (6)$$

where  $I_p$  is the oxidation peak current (A),  $A$  is the area of the electrode ( $\text{cm}^2$ ),  $C$  is the concentration of the electroactive species ( $= 0.01 \text{ M}$  of  $[\text{Fe}(\text{CN})_6]^{4-} + [\text{Fe}(\text{CN})_6]^{3-}$ ),  $n$  is the number of electrons transferred contributing to the redox reaction ( $= 1$  in this case),  $D$  is the diffusion coefficient, and  $\nu$  is the scan rate ( $\text{V s}^{-1}$ ).

The  $2e^-$  ORR activity and selectivity were evaluated by RRDE (5-mm glassy carbon disk, Pt ring) tests in 0.10 M  $\text{O}_2$ -saturated  $\text{Na}_2\text{SO}_4$  electrolyte. In RRDE experiments, the ring potential ( $E_{\text{ring}}$ ) was set to 1.54 V vs RHE. The  $\text{H}_2\text{O}_2$  selectivity (in %) and electron transfer number ( $n$ ) of the catalysts were determined based on the current of both disk ( $I_D$ ) and ring ( $I_R$ ) electrodes (Eqs. (7) and (8), respectively) [30].

$$\text{H}_2\text{O}_2(\%) = 200 \frac{I_R}{NI_D + I_R} \quad (7)$$

$$n = 4 \frac{I_D}{I_D + I_R/N} \quad (8)$$

where  $N$ , representing the empirical collection efficiency, was calculated by measuring the ratio between the ring limiting current and the disk

limiting current obtained from LSV tests in an  $N_2$ -saturated 10 mM  $K_3Fe(CN)_6 + 1$  M KCl solution, resulting in a value of  $N = 0.276$ .

### 2.5. Computational details

Structural modeling and DFT calculation were carried out using the Vienna ab initio simulation package (VASP), considering the generalized gradient approximation (GGA) and the Perdew-Burke-Ernzerhof (PBE) functional. To describe ionic cores, the projector augmented wave (PAW) pseudo-potentials were employed. A plane-wave basis set, with a kinetic-energy cut-off of 400 eV, was used to expand the wave function of valence electrons. Van der Waals interactions were described by means of the DFT-D3 empirical correction method. The geometry optimization was terminated once the force convergence was smaller than  $0.05$  eV  $\text{\AA}^{-1}$ . Monkhorst-Pack k-points of  $1 \times 1 \times 1$  were applied for all calculations.

## 3. Results and discussion

### 3.1. Characterization of PTFE/PMHS-GDE

Upon addition of a trace amount of PMHS, the hydroxyl groups on the CB surface react with the Si-H bonds to form Si-O-C moieties, thus ensuring a strong chemical bonding of PMHS chains to the electrode surface. This gives rise to a superhydrophobic interface that retains abundant Si-H and Si-O-C sites [35,40]. As a result of the introduction of low surface energy  $-CH_3$  groups of PMHS, the water contact angle of the electrode significantly increased from  $104.5^\circ$  to  $148.3^\circ$ , which could greatly favor the  $O_2$  permeation during the  $2e^-$  ORR (Fig. 1b). The cross-section SEM image of the PTFE/PMHS-GDE in Fig. 1c allows distinguishing a dense skin (top layer) with a thickness of about  $547.1 \mu\text{m}$ , which can be attributed to the PTFE- and PMHS-rich catalytic layer

immobilized on the carbon cloth. In addition, the SEM image of the surface in Fig. 1d shows a relatively smooth catalytic interface with several wrinkles, and the corresponding EDS-mapping reveals the uniform distribution of C, F, O and Si in the as-prepared GDE, suggesting the homogeneous dispersion of both polymers throughout the CB layer.

XPS analysis was performed to determine the chemical composition at the surface of GDEs with and without PMHS. Fig. 2a shows three peaks assigned to C 1s, O 1s and F 1s in the spectrum of PMHS-free GDE. The presence of O 1s is attributed to diverse oxygen functional groups, such as C-OH and  $C=O$ , formed on the surface of CB during the air thermal treatment, in addition to the intrinsic oxygen functionalities [45,46]. After the introduction of PMHS, new signals attributed to Si 2p and Si 2s emerged at 103.4 eV and 154.4 eV, respectively, whereas the peak intensity of O 1s dramatically increased. These results confirm the successful incorporation of PMHS onto the catalytic interface of the GDE. Note also that the peak intensity of O 1s is much higher than that of Si, which can be explained by the increased oxidation states of Si in the immobilized PMHS chains [40]. More specifically, the high-resolution C 1s spectrum of the PTFE/PMHS-GDE (Fig. 2b) has been deconvoluted into five peaks centered at 283.9, 284.8, 285.7, 286.7 and 292.4 eV, assigned to C-Si, C-C, C-O,  $C=O$  and C-F bonds, respectively. The former bond can be related to the  $-Si-CH_3$  of PMHS [47]. The deconvolution of the O 1s spectrum yields three peaks:  $C=O$ , C-O, and Si-O at 535.07, 534.03 and 533.29 eV, respectively (Fig. 2c) [48]. As mentioned above, the oxidation of CB gave rise to some oxygen functional groups, such as  $C=O$  and C-O, which can favor the adsorption of  $O_2$  molecules during ORR. Moreover, the characteristic Si 2p signal was deconvoluted into three peaks at 102.7, 103.5 and 104.4 eV, attributed to Si-H (18.34%), Si-C (54.05%) and Si-O (27.57%) bonds, respectively (Fig. 2d) [49]. The formation of Si-O bonds demonstrates the conversion of partial Si-H bonds to Si-O-C moieties during the synthesis, corroborating the tight chemical attachment of PMHS in the catalytic layer.

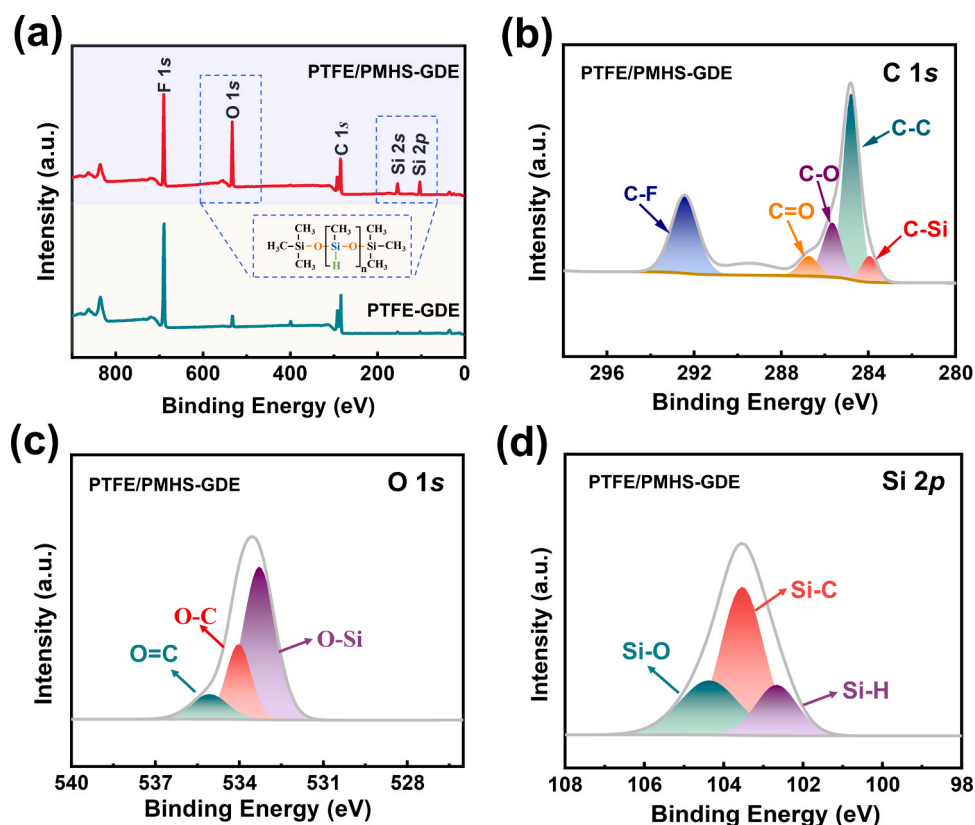


Fig. 2. (a) XPS full spectra of conventional PTFE/GDE and novel PTFE/PMHS-GDE. High-resolution XPS spectra of (b) C 1s, (c) Si 2p, and (d) O 1s of PTFE/PMHS-GDE.



### 3.2. Electrocatalytic ORR activity of PTFE/PMHS-GDE

First, the cyclic voltammograms for the  $[\text{Fe}(\text{CN})_6]^{3-}/[\text{Fe}(\text{CN})_6]^{4-}$  redox system were recorded to evaluate the electrochemically active surface area (ECSA) of the synthesized materials. As illustrated in Fig. 3a, the CB-PTFE electrocatalyst had slightly greater oxidation and reduction peak current densities (see also Table S1), which led to a slightly higher area than the CB-PTFE/PMHS ( $8.3$  vs  $7.5$   $\text{cm}^2$ ). The ECSA represents the area that is accessible to the electrolyte and hence, it can be concluded that the great increase of hydrophobicity (Fig. 1b) caused by PHMS leads to a smaller contact between the catalytic layer and electrolyte [16]. Nonetheless, the formation of the superhydrophobic three-phase boundary turned out to be beneficial for the ORR thanks to the enhanced  $\text{O}_2$  permeability, as will be demonstrated below.

Further analysis of the electron/ion transport behavior of the GDEs was conducted by electrochemical impedance spectroscopy (EIS). The Nyquist plots shown in Fig. 3b were fitted to an equivalent circuit model, yielding the values of mass transport resistance ( $R_{\text{mt}}$ ) and charge transfer resistance ( $R_{\text{ct}}$ ). Surprisingly, the introduction of a trace amount of PMHS into the CB-PTFE gave rise to extremely low  $R_{\text{mt}}$  and  $R_{\text{ct}}$  values.

The abundant  $-\text{CH}_3$  groups in PHMS created a hydrophobic interface without significant destruction of the porous structures, which is excellent for promoting the  $\text{O}_2$  transport. Moreover, the Si-H and Si-O-C bonds arising from PHMS incorporation may accelerate the electron transfer on the catalytic interface, leading to the reduction of  $R_{\text{ct}}$ . Consequently, the CB-PTFE/PMHS particles displayed much lower  $R_{\text{mt}}$  and  $R_{\text{ct}}$  values ( $23.6$  and  $3.8$   $\text{k}\Omega$ ) than the CB-PTFE ( $47.5$  and  $7.6$   $\text{k}\Omega$ ), demonstrating the enhancement of both mass and electron transports (Table S1). Fig. 3c displays the linear sweep voltammograms of five catalysts with different PMHS content for ORR in  $0.05$  M  $\text{Na}_2\text{SO}_4$  aqueous solution. The catalyst with a PHMS/PTFE mass ratio of  $0.038$  exhibited excellent ORR performance, reaching the most positive onset potential ( $0.56$  V vs RHE) and the highest cathodic current density ( $-0.42$   $\text{mA cm}^{-2}$  at  $-0.4$  V vs RHE). Meanwhile, the catalysts with PMHS/PTFE ratios of  $0$ ,  $0.019$ ,  $0.075$  and  $0.125$  achieved more negative onset potentials of  $0.36$ ,  $0.48$ ,  $0.47$ ,  $0.45$  V vs RHE and lower current densities of  $-0.20$ ,  $-0.30$ ,  $-0.36$ ,  $-0.28$   $\text{mA cm}^{-2}$ , respectively. As reported, the current response would be suppressed as the amount of hydrophobic binder is increased, since it can partially block active sites of CB for ORR [24]. In contrast, the introduction of an appropriate

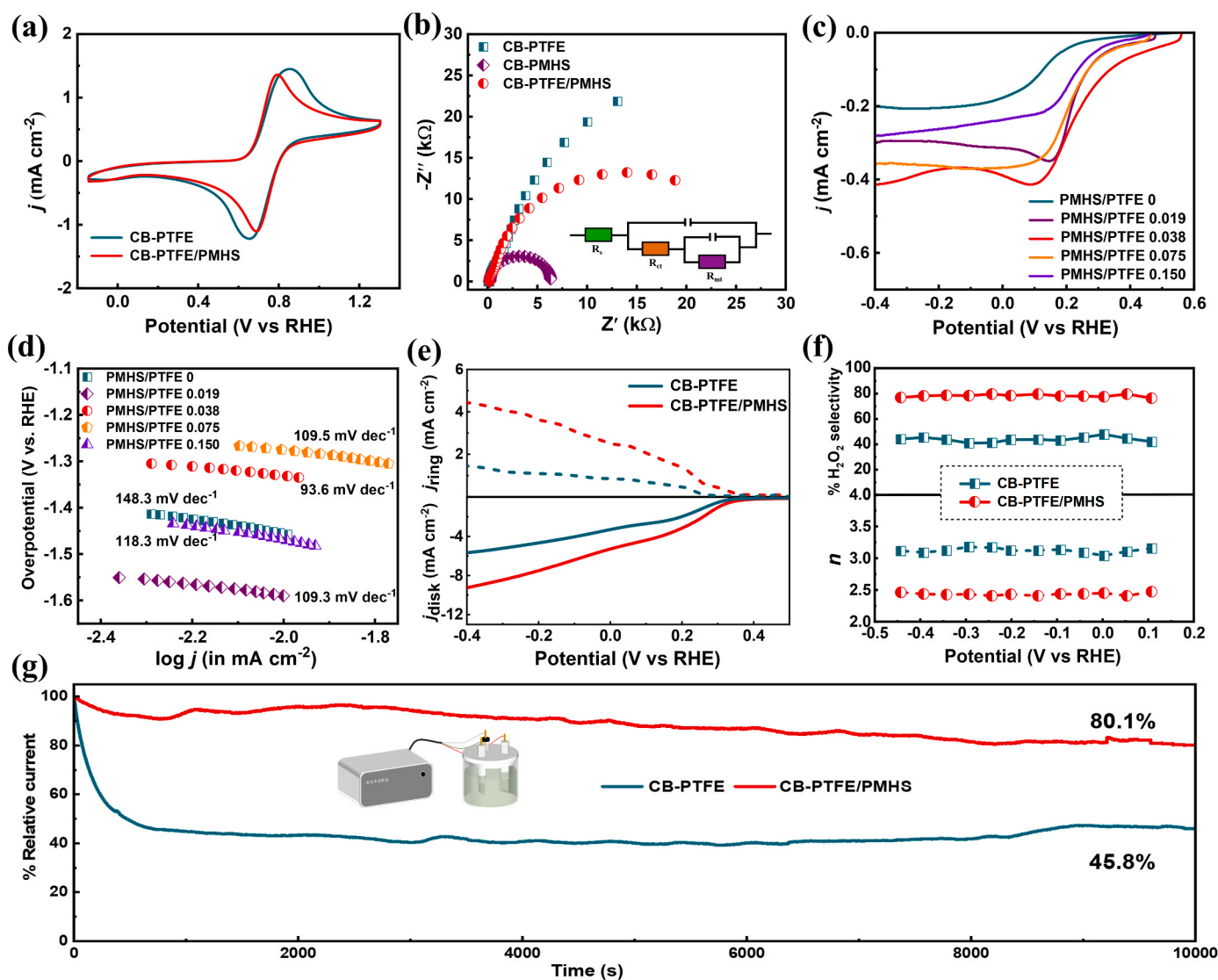


Fig. 3. Electrochemical tests of different catalysts. (a) Cyclic voltammograms obtained in  $0.01$  M  $[\text{Fe}(\text{CN})_6]^{3-} + 0.01$  M  $[\text{Fe}(\text{CN})_6]^{4-}$  solution at pH 5.2; (b) Nyquist plots; (c) linear sweep voltammograms in  $0.05$  M  $\text{Na}_2\text{SO}_4$  solution, and (d) corresponding Tafel plot; (e) RRDE tests in  $\text{O}_2$ -saturated  $0.1$  M  $\text{Na}_2\text{SO}_4$  at pH 6.1 at a scan rate of  $10$   $\text{mV s}^{-1}$  ( $E_{\text{ring}} = 1.54$  V vs RHE), and (f) the corresponding  $\text{H}_2\text{O}_2$  selectivity and electron transfer number ( $n$ ). and (g) chronoamperometric responses for CB-PTFE and CB-PTFE/PMHS.

amount of PMHS is proven positive. This behaviour agrees with the enhanced mass and charge transfer determined from EIS analysis, attributable to the new Si-H and Si-O-C functional groups that favor the  $2e^-$  ORR. At an excessively high PMHS content, the ORR is gradually inhibited due to the reduction of exposed active sites. From these voltammograms, the corresponding Tafel plots for the different catalysts are illustrated in Fig. 3d. A lower Tafel slope suggests a faster electrode reaction at constant operation conditions. As can be observed, the results are consistent with the previous LSV tests, since the smallest Tafel slope of  $93.6 \text{ mV dec}^{-1}$  was achieved with the PMHS/PTFE ratio of 0.038, implying the best electrochemical performance. Therefore, it can be concluded that the ORR activity of conventional CB/PTFE cathodes can be substantially improved upon simple modification with an appropriate amount of PMHS.

The ORR performance of CB-PTFE and CB-PTFE/PMHS electrocatalysts was further evaluated in  $\text{O}_2$ -saturated  $0.1 \text{ M Na}_2\text{SO}_4$  electrolyte using an RRDE at a rotation rate of 1600 rpm. Fig. 3e displays the polarization curves of the two materials, including the  $\text{O}_2$  reduction currents detected on the disk (solid lines) and the  $\text{H}_2\text{O}_2$  oxidation currents measured on the ring (dashed lines). At the disk, much higher current and more positive reduction potential were obtained using the CB-PTFE/PMHS, confirming the enhanced ORR kinetics, in good agreement with the results of Tafel plots. In addition to the higher ORR activity, the electron transfer number calculated from the RRDE results for CB-PTFE/PMHS was around 2.4 (Fig. 3f), which was close to the theoretical value ( $n = 2$ ) required for  $\text{H}_2\text{O}_2$  formation. The electron transfer number increased to around 3.1 for CB-PTFE. The corresponding  $\text{H}_2\text{O}_2$  selectivity for the CB-PTFE/PMHS was around 80%, being superior to that of CB/PTFE (less than 45% on average). In addition, even after subjecting the electrode to about 3 h of continuous chronoamperometric measurement at  $-0.1 \text{ V}$ , the current density at CB-PTFE/PMHS remained above 80.0%, being much higher than that at CB-PTFE

(45.8%) (Fig. 3g). This significant difference underscores the robust catalytic ability of CB-PTFE/PMHS. Therefore, the activity, selectivity, and stability towards the  $2e^-$  ORR were significantly improved by the introduction of a low amount of PMHS, as a result of the better  $\text{O}_2$  mass transport and electron transfer.

### 3.3. Electrochemical $\text{H}_2\text{O}_2$ accumulation and durability tests

A demonstration of the presumed superiority of as-prepared PTFE/PMHS-GDE for  $\text{H}_2\text{O}_2$  production was carried out in an undivided cell with an  $\text{IrO}_2$ -based anode. Prior to this, the accumulation of  $\text{H}_2\text{O}_2$  concentration using conventional PTFE-GDEs with different PTFE/CB mass ratios was determined to optimize the PTFE loading (Fig. S1a). The optimal PTFE/CB ratio was found to be 1, since it yielded a remarkable  $\text{H}_2\text{O}_2$  production of  $1483.7 \text{ mg L}^{-1}$ , whereas further rise the PTFE content proved to be detrimental. The water contact angle of the cathode surface gradually increased from  $94.3^\circ$  to  $128.5^\circ$  when the PTFE/CB ratio was risen from 1 to 5 (Fig. S2a), in agreement with the greater hydrophobicity of the GDE interface that is expected to enhance the  $\text{O}_2$  permeability. However, the number of active sites decreased concomitantly due to the agglomeration of PTFE during the sintering process [24,50]. On the other hand, despite the outstanding  $\text{H}_2\text{O}_2$  synthesis performance of the GDEs with PTFE/CB ratios of 1 and 2, such low PTFE loadings resulted in the easy collapse of the catalytic layer, which was structurally unstable in the absence of a greater amount of binder that could sustain the CB particles. Therefore, a moderate PTFE/CB ratio of 3 was selected to provide a sufficient number of stable pore channels for rapid  $\text{O}_2$  transport, without compromising the electron transfer, as proven by the good  $\text{H}_2\text{O}_2$  accumulation of up to  $1087.4 \text{ mg L}^{-1}$  at 360 min. Based on this and the result discussed in Fig. 3c, the performance of a PTFE/PMHS-GDE fabricated with the optimized PTFE loading and a PMHS/PTFE ratio of 0.038 was evaluated. As depicted in

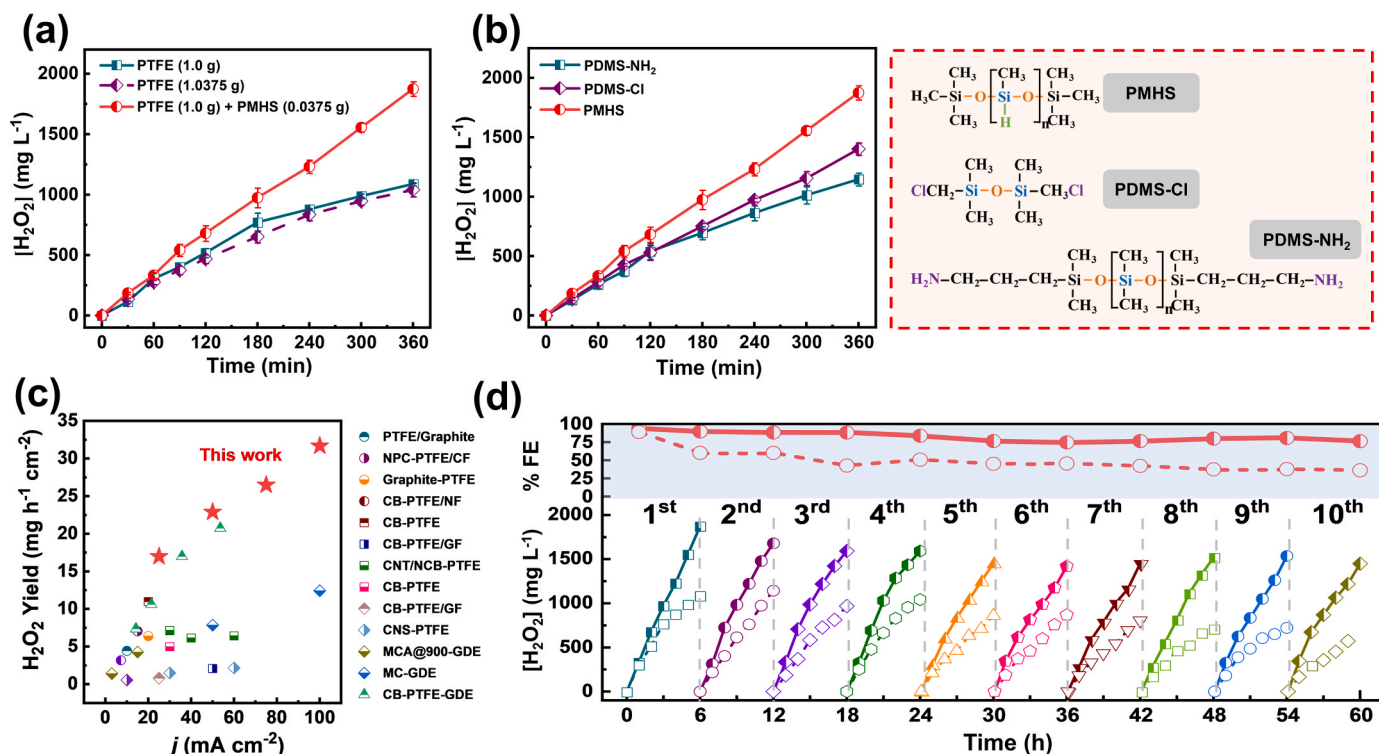


Fig. 4. (a) Comparison of  $\text{H}_2\text{O}_2$  concentration profiles using conventional two GDEs with different PTFE loadings and a novel PTFE/PMHS-GDE, in  $0.05 \text{ M Na}_2\text{SO}_4$  at pH 6.1 and  $25.0 \text{ mA cm}^{-2}$ . (b)  $\text{H}_2\text{O}_2$  concentration profiles using siloxane-modified GDEs (see structures of the modifiers), under the same conditions described in plot (a). (c) Comparison of the  $\text{H}_2\text{O}_2$  yield at different current densities with values reported in the literature for carbonaceous cathodes [4,12,25,26,51–57]. (d) Stability test performed with the PTFE-GDE (dashed curves) and the PTFE/PMHS-GDE (solid curves) in ten consecutive runs, each of 6 h duration, in  $0.05 \text{ M Na}_2\text{SO}_4$  at pH 6.1 and  $25 \text{ mA cm}^{-2}$ .

Fig. 4a, the accumulated  $\text{H}_2\text{O}_2$  concentration was excellent, attaining up to  $1874.8 \text{ mg L}^{-1}$  after 360 min, being much higher than that attained with a conventional PTFE-GDE ( $1087.4 \text{ mg L}^{-1}$ ). In addition, another GDE was fabricated employing an equivalent amount of PTFE to substitute PMHS, but the result was similar to the latter GDE (Fig. 4a), which corroborates the indispensable role of PMHS in boosting  $\text{H}_2\text{O}_2$  production.

Aiming to further highlight the relevance of the Si-H bonds, poly(dimethylsiloxane)etherimide (PDMS-NH<sub>2</sub>) and 1,3-bis-(dichloromethyl)-1,1,3,3-tetramethyldisiloxane (PDMS-Cl) with similar molecular structures but different functional groups (see Fig. 4b) were used to prepare modified GDEs, following the same fabrication procedure. As shown in Fig. 4b, the  $\text{H}_2\text{O}_2$  concentrations accumulated with the PDMS-NH<sub>2</sub>-GDE and PDMS-Cl-GDE were  $1145.9$  and  $1401.1 \text{ mg L}^{-1}$  at 360 min, respectively, being slightly higher than that attained with the conventional PTFE-GDE but much lower than using the PTFE/PMHS-GDE. These results demonstrate the crucial role of the electron-withdrawing Si-H bonds in the enhancement of  $\text{H}_2\text{O}_2$  generation.

The effect of several experimental parameters, including relative PMHS content, solution pH, and current density on the  $\text{H}_2\text{O}_2$  concentration profiles was investigated. The final accumulation of  $\text{H}_2\text{O}_2$  was substantially improved from  $1345.0$  to  $1874.8 \text{ mg L}^{-1}$  with an appropriate increase in the PMHS/PTFE ratio from 0.019 to 0.038, whereas higher loadings of PMHS significantly hampered the  $\text{H}_2\text{O}_2$  generation (Fig. S1b). This observation is consistent with the maximum water contact angle ( $148.3^\circ$ ) measured at the PMHS/PTFE ratio of 0.038 (Fig. S2b). A low-to-moderate PMHS loading allows the creation of a superhydrophobic interface that ensures an efficient  $\text{O}_2$  supply and the presence of new active sites, but an excess of PMHS significantly decreases the surface hydrophobicity, consequently hindering the  $\text{O}_2$  transport. As reported, redundant PMHS can fill the surface concave regions, resulting in a decrease in surface roughness. Note that this kind of correlation between the contact angle and surface roughness has been described for a hydrophobic surface [40]. These findings fully agree with the results presented in Figs. 3c and 3d. The effect of solution pH, between 3.0 and 11.0, on the accumulated  $\text{H}_2\text{O}_2$  concentration using the PTFE/PMHS-GDE was studied as well. As depicted in Fig. S1c, the  $\text{H}_2\text{O}_2$  accumulation was very high ( $1487.6$ – $1874.8 \text{ mg L}^{-1}$ ) within a wide pH range from 3.0 to 9.0, whereas its values dramatically dropped off to  $794.4 \text{ mg L}^{-1}$  after 360 min at pH 11.0. This decrease can be attributed to the rapid decomposition of  $\text{H}_2\text{O}_2$  via the disproportionation Reactions (9) and (10), and the lack of protons required for  $\text{H}_2\text{O}_2$  electrosynthesis in such a strong alkaline environment [12].



Current density also has a significant influence on  $\text{H}_2\text{O}_2$  production. Fig. 4c shows the  $\text{H}_2\text{O}_2$  yields using the PTFE/PMHS-GDE at different current densities up to  $100 \text{ mA cm}^{-2}$ , as compared to results reported in the literature for  $\text{H}_2\text{O}_2$  accumulation with GDEs. It can be observed that the new PTFE/PMHS-GDE exhibits the best  $2e^-$  ORR performance among all the GDEs, and the  $\text{H}_2\text{O}_2$  productivities were progressively enhanced as the applied current was increased. Worth noticing, the  $\text{H}_2\text{O}_2$  accumulation was only slightly improved or even inhibited with other GDEs at high current density, which has been usually explained from competitive parasitic reactions, such as the  $4e^-$  ORR, hydrogen evolution reaction and cathodic  $\text{H}_2\text{O}_2$  decomposition [12]. Consequently, most of the reported  $2e^-$  ORR systems based on GDEs exhibited a dramatic decay of Faradaic efficiency at elevated current density, making them unsuitable for industrial application [58]. In contrast, the PTFE/PMHS-GDE displayed only a slight decrease in efficiency, from 100% to 82.2%, as the current density increased from 25 to  $100 \text{ mA cm}^{-2}$ , demonstrating the high activity and selectivity of the PTFE/PMHS-GDE towards the  $\text{H}_2\text{O}_2$  electrosynthesis even at demanding conditions (Fig. S3). This finding is very inspiring and favorable for the

industrial scale-up of electrochemical devices, since they frequently require cathodes that can work at high current density.

To inspect the long-term durability of the PTFE/PMHS-GDE, ten consecutive  $\text{H}_2\text{O}_2$  production trials (each cycle prolonged for 6 h) were conducted at  $25 \text{ mA cm}^{-2}$ . As depicted in Fig. 4d, the accumulated  $\text{H}_2\text{O}_2$  concentration was kept at high levels ranging between  $1874.8$  and  $1449.3 \text{ mg L}^{-1}$ , accounting for a 22.7% decrease as maximum after the 10 runs. Accordingly, this was accompanied by very high faradaic efficiencies ranging from 89.7% to 76.2%. The decay in performance is attributed to the imbalance between gas and liquid supply to the active sites of the GDE as the electrolysis is prolonged. This causes the gradual flooding of the pores by electrolyte penetration, inactivating some of the catalytic sites upon lack of sufficient  $\text{O}_2$  permeation [20]. Despite the observed decline in performance over prolonged exposure, the long-term running performance was superior to that of the PTFE-GDE, which suffered from more severe reductions in both  $\text{H}_2\text{O}_2$  accumulation (36.5% decrease) and faradaic efficiency (from 89.1% to 36.1%). Additionally, the contact angle of the PMHS-modified cathode underwent only a slight decrease from  $148.3^\circ$  to  $125.5^\circ$  after the consecutive runs, still surpassing that of PTFE-GDE. The preserved superhydrophobic surface ensured efficient  $\text{O}_2$  diffusion (Fig. S4). Overall, these results confirm the promising long-term stability of the PTFE/PMHS-GDE, exhibiting great potential for larger-scale  $\text{H}_2\text{O}_2$  electrosynthesis.

### 3.4. EF treatment of micropollutants with the PTFE/PMHS-GDE

Once demonstrated that the PTFE/PMHS-GDE is able to boost the  $\text{H}_2\text{O}_2$  production and perform very well for a long period, its feasibility to conduct the EF treatment of eight target organic micropollutants widely detected in water streams was evaluated. Prior to this, the effect of  $\text{Fe}^{2+}$  dosage and current density on the EF performance was evaluated for 60 min using a solution containing  $20.0 \text{ mg L}^{-1}$  2,4-dichlorophenol (2,4-DCP). As can be seen in Fig. 5a, the decay of 2,4-DCP was enhanced at gradually higher  $\text{Fe}^{2+}$  dosage, and its total disappearance could be achieved in only 50 min employing 0.2 and 0.3 mM  $\text{Fe}^{2+}$ . As shown in the inset, the pseudo-first-order rate constant increased (from  $0.028$  to  $0.095 \text{ min}^{-1}$ ) as the  $\text{Fe}^{2+}$  dosage rose from 0.1 to 0.3 mM. Since abundant  $\text{H}_2\text{O}_2$  can be produced in this EF system, the increase in  $\text{Fe}^{2+}$  dosage favors the Fenton's reaction, eventually yielding a higher amount of hydroxyl radical ( $\bullet\text{OH}$ ) that accelerate the 2,4-DCP degradation. Similarly, the increase in current density also showed a positive influence, as deduced from Fig. 5b. A significant enhancement in the degradation rate constant, from  $0.037$  to  $0.117 \text{ min}^{-1}$  was achieved when increasing the current density from  $12.5$  to  $37.5 \text{ mA cm}^{-2}$ . Conversely, at  $50.0 \text{ mA cm}^{-2}$ , the improvement was minor, due to the fact that an excessively high  $\text{H}_2\text{O}_2$  concentration partly scavenges the  $\bullet\text{OH}$  [59]. The degradation of other micropollutants was then carried out with  $0.20 \text{ mM Fe}^{2+}$  at  $25 \text{ mA cm}^{-2}$ . Fig. 5c shows that around 90% removal of each micropollutant (except 2,4-DCP and DCF) can be obtained in only 20 min using the PTFE/PMHS-GDE. Its performance was superior to that of EF with a conventional PTFE-GDE in all the cases, in good agreement with the previous characterization of the GDEs. The low degradation efficiencies for 2,4-DCP and diclofenac sodium (DCF) solutions are explained by their specific molecular structures, which may be more resistant to  $\bullet\text{OH}$  attack [60]. Moreover, the residual  $\text{H}_2\text{O}_2$  concentrations after the treatment with PTFE/PMHS-GDE were much higher. Overall, these results demonstrate the great potential of the PTFE/PMHS-GDE as the cathode in EF system for wastewater treatment.

### 3.5. Mechanistic insights

To gain an in-depth understanding of the role of PMHS in the enhancement of the  $2e^-$  ORR, DFT calculations were performed. This allowed determining the Gibbs free energies of each elementary step of the ORR, as well as the charge distributions on the coordination



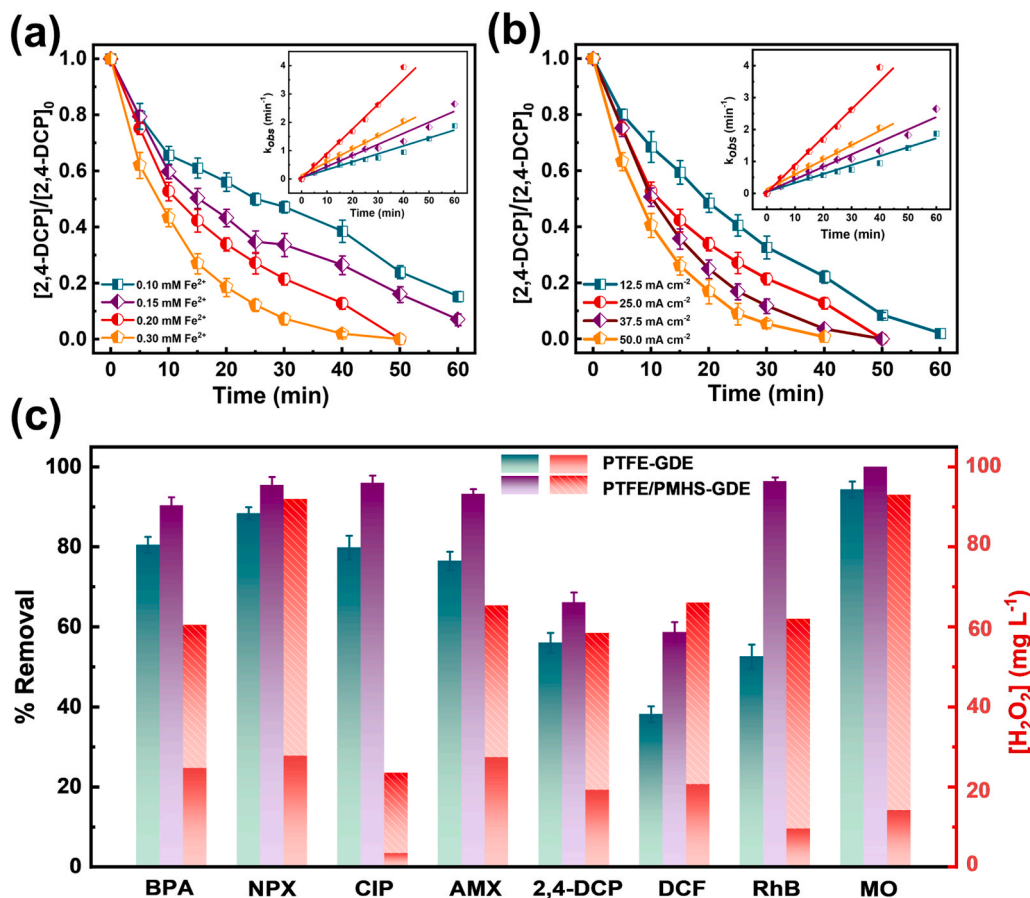


**Fig. 5.** Effect of (a)  $\text{Fe}^{2+}$  dosage and (b) applied current density on the decay of 2,4-dichlorophenol (2,4-DCP) during EF process using a PTFE/PMHS-GDE. In the insets, the corresponding pseudo-first-order kinetic analysis is illustrated. (c) Micropollutant removals and residual  $\text{H}_2\text{O}_2$  concentrations achieved after 20 min of EF treatment using the conventional PTFE-GDE and the novel PTFE/PMHS-GDE. Conditions for trials in plot (c): [Micropollutant] = 20  $\text{mg L}^{-1}$ ;  $[\text{Fe}^{2+}] = 0.20 \text{ mM}$ ; initial pH 3.0; current density = 25  $\text{mA cm}^{-2}$ . Micropollutants: bisphenol A (BPA), naproxen (NPX), ciprofloxacin (CIP), amoxicillin (AMX), diclofenac sodium (DCF), Rhodamine B (RhB), Methyl Orange (MO) and 2,4-DCP.

structures of sole graphene and PMHS@Graphene. As shown in Fig. 6a, the  $2e^-$  ORR pathway producing  $\text{H}_2\text{O}_2$  competes with the  $4e^-$  reaction pathway. Specifically, the former consists of two steps, namely the generation and removal of the  $^*\text{OOH}$  intermediate, while the cleavage of the O-O bond in  $^*\text{OOH}$  to produce  $^*\text{O}$  and  $^*\text{OH}$  as intermediates gives rise to the  $4e^-$  route [28]. Therefore, the key to minimize the latter is to prevent the dissociation of the O-O bond in  $^*\text{OOH}$ . As depicted in the free energy diagram calculated at 0 V vs RHE (Fig. 6b), the formation of  $^*\text{OOH}$  via an endothermic  $\text{O}_2$  hydrogenation step is uphill, whereas other steps remain downhill for the materials under consideration, implying that it is the potential limiting step [61]. The Gibbs free energy difference of this step ( $\Delta G_{^*\text{OOH}}$ ) on PMHS@Graphene is much lower than that on sole graphene (0.02 vs 0.23 eV), demonstrating that the presence of PMHS favors the  $^*\text{OOH}$  generation. On the other hand, the free energy change for the conversion of  $^*\text{OOH}$  to  $^*\text{O}$  ( $\Delta G_{^*\text{O}}$ ) on sole graphene is  $-2.93 \text{ eV}$ , much more negative than  $-1.80 \text{ eV}$  for the  $\text{H}_2\text{O}_2$  formation ( $\Delta G_{\text{H}_2\text{O}_2}$ ), suggesting that the  $2e^-$  ORR on this material is suppressed. Regarding the PMHS@Graphene electrocatalyst, the  $\Delta G_{^*\text{O}}$  becomes much more positive ( $-1.86 \text{ eV}$ ) than that of graphene, while the  $\Delta G_{\text{H}_2\text{O}_2}$  remains very similar (1.60 vs 1.80 eV), thereby corroborating that the presence of PMHS significantly inhibits the  $4e^-$  ORR pathway by preserving the  $^*\text{OOH}$  intermediate from dissociation without sacrificing the  $2e^-$  ORR activity. Moreover, more insights into the role of the Si-H and Si-O-C groups in the enhancement of the  $2e^-$  ORR were provided by investigating the  $^*\text{OOH}$  adsorption free energy on three different sites. The  $^*\text{OOH}$  adsorption largely determines the ORR and hence, the free energy for ideal  $2e^-$  ORR is 3.52 eV at the

equilibrium potential of 0.70 V vs RHE [22]. As shown in Fig. 6c, the Si-H site has a free energy of 4.41 eV, being the closest to the ideal value, which means that the weakest adsorption of  $^*\text{OOH}$  occurred on this site. The free energy on the Si-O-C site is also slightly more negative than that on the C site in PMHS@Graphene, suggesting its positive contribution to the  $2e^-$  ORR. On the other hand, the charge density analysis depicted in Fig. 6d reveals that the electrons tend to accumulate around the Si sites in PMHS, which modulated the local electric field of C sites in graphene, resulting in moderate charge transfer. These DFT results demonstrate that the Si-H and Si-O-C sites cannot only act as the active sites for the  $2e^-$  ORR, but they also promote electron transfer during the reaction.

#### 4. Conclusions

In summary, a highly hydrophobic PTFE/PMHS-GDE that can simultaneously enhance the  $\text{O}_2$  transport,  $\text{H}_2\text{O}_2$  selectivity, and catalytic activity, has been rationally developed, thereby significantly improving the  $\text{H}_2\text{O}_2$  yield as compared to other reported GDEs. The  $-\text{CH}_3$  groups in PMHS, with low surface energy, create a superhydrophobic three-phase interface that eliminates the  $\text{O}_2$  mass transport barrier for ORR, whereas the Si-H bonds and the as-formed Si-O-C sites modulate the coordination environment of carbon centers, achieving faster electron transfer and higher  $\text{H}_2\text{O}_2$  selectivity. Consequently, the PTFE/PMHS-GDE yields the maximum  $\text{H}_2\text{O}_2$  concentration of 1874.8  $\text{mg L}^{-1}$  after 360 min at 25  $\text{mA cm}^{-2}$ , being much higher than that of a conventional GDE. Moreover, the enhancement of EF system for wastewater treatment using the PTFE/PMHS-GDE was confirmed by the efficient degradation



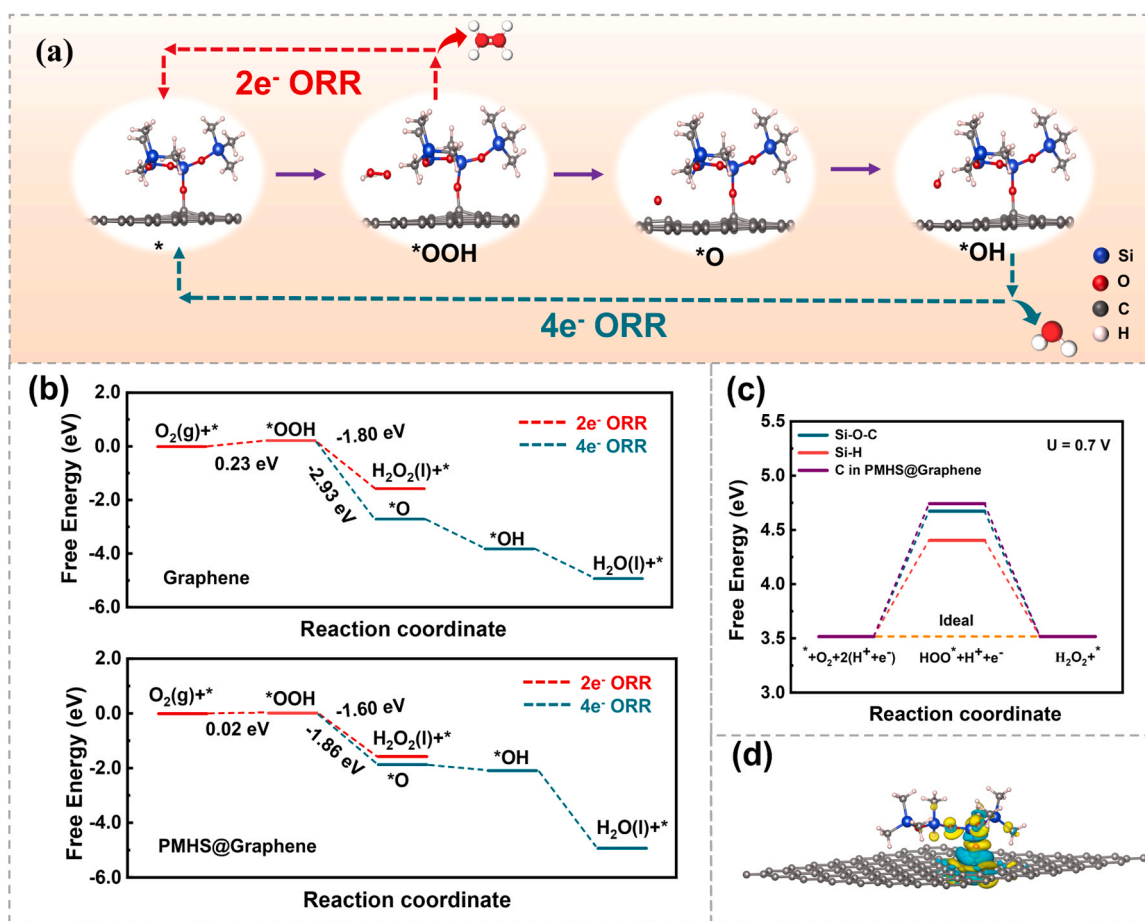


**Fig. 6.** (a) Possible reaction pathways during the ORR. (b) Gibbs free energy diagram for  $2e^-$  and  $4e^-$  ORR on sole graphene and PMHS@Graphene centers at 0 V vs RHE. (c) Free energy diagram for  $2e^-$  ORR to  $H_2O_2$  at equilibrium potential of 0.70 V vs RHE. (d) Charge density difference in the PMHS@Graphene model (the azure regions denote charge depletion, whereas yellow regions denote charge accumulation).

of 8 micropollutants. This study is expected to exert a positive impact on EF systems that are designed by many scholars and, beyond this, the positive effects of the active sites in PMHS may serve to fabricate novel GDEs with better performance in other fields, such as electrochemical CO<sub>2</sub> reduction.

#### CRedit authorship contribution statement

**Pan Xia:** Conceptualization, Data curation, Investigation, Validation; **Lele Zhao:** Investigation, Formal analysis; **Xi Chen:** Data curation, Investigation; **Zhihong Ye:** Conceptualization, Funding acquisition, Investigation, Methodology, Project administration, Resources, Supervision, Writing – original draft; **Zhihong Zheng:** Data curation, Formal analysis; **Qiang He:** Resources, Supervision; **Ignasi Sirés:** Funding acquisition, Methodology, Project administration, Resources, Supervision, Writing – review & editing.

#### Declaration of Competing Interest

The authors declare that they have no known competing financial interests or personal relationships that could have appeared to influence the work reported in this paper.

#### Data availability

Data will be made available on request.

#### Acknowledgments

The authors acknowledge financial support from the National Natural Science Foundation of China (No.52100073), the PhD Gateway Program of Chongqing, (CSTB2022BSXM-JCX0140), the Graduate Scientific Research and Innovation Foundation of Chongqing (CYB23065), the Natural Science Foundation of Chongqing, (CSTB2022NSCQ-MSX0432) and the Venture and Innovation Support Program for Chongqing Over-seas Returnees (cx2022048, China). I.S. is thankful to projects PID2019-109291RB-I00, PID2022-140378OB-I00 and PDC2022-133624-I00 (MCIN/AEI/10.13039/501100011033, Spain). The Ph.D. scholarship awarded to L.Z. (State Scholarship Fund, CSC, China) is also acknowledged.

#### Appendix A. Supporting information

Supplementary data associated with this article can be found in the online version at [doi:10.1016/j.apcatb.2023.123467](https://doi.org/10.1016/j.apcatb.2023.123467).

#### References

- [1] R. Mehrotra, D. Oh, J.W. Jang, Unassisted selective solar hydrogen peroxide production by an oxidised buckypaper-integrated perovskite photocathode, *Nat. Commun.* 12 (2021) 1–9.
- [2] H. Li, P. Wen, D.S. Itanze, Z.D. Hood, S. Adhikari, C. Lu, X. Ma, L. Dun, L. Jiang, D. L. Carroll, Y. Qiu, S.M. Geyer, Scalable neutral H<sub>2</sub>O<sub>2</sub> electro-synthesis by platinum diphosphide nanocrystals by regulating oxygen reduction reaction pathways, *Nat. Commun.* 11 (2020) 1–12.

- [3] C.A. Martínez-Huitile, M.A. Rodrigo, I. Sirés, O. Scialdone, A critical review on latest innovations and future challenges of electrochemical technology for the abatement of organics in water, *Appl. Catal. B: Environ.* 328 (2023), 122430.
- [4] Y. Zhang, G. Daniel, S. Lanzalaco, A.A. Isse, A. Facchin, A. Wang, E. Brillas, C. Durante, I. Sirés, H<sub>2</sub>O<sub>2</sub> production at gas-diffusion cathodes made from agarose derived carbons with different textural properties for acetubutol degradation in chloride media, *J. Hazard. Mater.* 423 (2022), 127005.
- [5] G. Ren, S. Lanzalaco, M. Zhou, P.L. Cabot, E. Brillas, I. Sirés, Replacing carbon cloth by nickel mesh as substrate for air-diffusion cathodes: H<sub>2</sub>O<sub>2</sub> production and carbencillin degradation by photoelectro-Fenton, *Chem. Eng. J.* 454 (2023), 140515.
- [6] Q. Wu, J. Cao, X. Wang, Y. Liu, Y. Zhao, H. Wang, Y. Liu, H. Huang, F. Liao, M. Shao, Z. Kang, A metal-free photocatalyst for highly efficient hydrogen peroxide photoproduction in real seawater, *Nat. Commun.* 12 (2021) 1–10.
- [7] X. Zhao, Q. Yin, X. Mao, C. Cheng, L. Zhang, L. Wang, T. Liu, Y. Li, Y. Li, Theory-guided design of hydrogen-bonded cobaltporphyrin frameworks for highly selective electrochemical H<sub>2</sub>O<sub>2</sub> production in acid, *Nat. Commun.* 13 (2022) 1–8.
- [8] I. Sirés, E. Brillas, Upgrading and expanding the electro-Fenton and related processes, *Curr. Opin. Electrochem.* 27 (2021), 100686.
- [9] N. Oturan, J. Bo, C. Trelu, M.A. Oturan, Comparative performance of ten electrodes in electro-Fenton process for removal of organic pollutants from water, *ChemElectroChem* 8 (2021) 3294–3303.
- [10] P. Xia, Z. Ye, L. Zhao, Q. Xue, S. Lanzalaco, Q. He, X. Q. I. Sirés, Tailoring single-atom FeN<sub>4</sub> moieties as a robust heterogeneous catalyst for high-performance electro-Fenton treatment of organic pollutants, *Appl. Catal. B: Environ.* 322 (2023), 122116.
- [11] J. Lu, X. Liu, Q. Chen, J. Zhou, Coupling effect of nitrogen-doped carbon black and carbon nanotube in assembly gas diffusion electrode for H<sub>2</sub>O<sub>2</sub> electro-generation and recalcitrant pollutant degradation, *Sep. Purif. Technol.* 265 (2021), 118493.
- [12] G.O.S. Santos, P.J.M. Cordeiro-Junior, I. Sánchez-Montes, R.S. Souto, M.S. Kronka, M.R.V. Lanza, Recent advances in H<sub>2</sub>O<sub>2</sub> electro-synthesis based on the application of gas diffusion electrodes: challenges and opportunities, *Curr. Opin. Electrochem.* 36 (2022), 101124.
- [13] W. Zhou, L. Rajic, X. Meng, R. Nazari, Y. Zhao, Y. Wang, J. Gao, Y. Qin, A. N. Alshawabkeh, Efficient H<sub>2</sub>O<sub>2</sub> electrogeneration at graphite felt modified via electrode polarity reversal: Utilization for organic pollutants degradation, *Chem. Eng. J.* 364 (2019) 428–439.
- [14] Y. Song, A. Wang, S. Ren, Y. Zhang, Z. Zhang, Flow-through heterogeneous electro-Fenton system using a bifunctional FeOCl/carbon cloth/activated carbon fiber cathode for efficient degradation of trimethoprim at neutral pH, *Environ. Res.* 222 (2023), 115303.
- [15] H. Zhang, Y. Zhao, Y. Li, G. Li, J. Li, F. Zhang, Janus electrode of asymmetric wettability for H<sub>2</sub>O<sub>2</sub> production with highly efficient O<sub>2</sub> utilization, *ACS Appl. Mater. Inter.* 3 (2019) 705–714.
- [16] P. Cao, X. Quan, K. Zhao, X. Zhao, S. Chen, H. Yu, Durable and selective electrochemical H<sub>2</sub>O<sub>2</sub> synthesis under a large current enabled by the cathode with highly hydrophobic three-phase architecture, *ACS Catal.* 11 (2021) 13797–13808.
- [17] Y. Li, C.J. Miller, L. Wu, T.D. Waite, Hydroxyl radical production via a reaction of electrochemically generated hydrogen peroxide and atomic hydrogen: An effective process for contaminant oxidation? *Environ. Sci. Technol.* 56 (2022) 5820–5829.
- [18] F. Deng, J. Jiang, I. Sirés, State-of-the-art review and bibliometric analysis on electro-Fenton process, *Carbon Lett.* 33 (2023) 17–34.
- [19] J. An, N. Li, Y. Wu, S. Wang, C. Liao, Q. Zhao, L. Zhou, T. Li, X. Wang, Y. Feng, Revealing decay mechanisms of H<sub>2</sub>O<sub>2</sub>-based electrochemical advanced oxidation processes after long-term operation for phenol degradation, *Environ. Sci. Technol.* 54 (2020) 10916–10925.
- [20] A. Xu, B. He, H. Yu, W. Han, J. Li, J. Shen, X. Sun, L. Wang, A facile solution to mature cathode modified by hydrophobic dimethyl silicon oil (DMS) layer for electro-Fenton processes: Water proof and enhanced oxygen transport, *Electrochim. Acta* 308 (2019) 158–166.
- [21] M.E. Leonard, L.E. Clarke, A. Forner-Cuenca, S.M. Brown, F.R. Brushett, Investigating electrode flooding in a flowing electrolyte, gas-fed carbon dioxide electrolyzer, *ChemSusChem* 13 (2020) 400–411.
- [22] Y. Zheng, X. Xu, J. Chen, Q. Wang, Surface O<sub>2</sub>-regulation on POM electrocatalyst to achieve accurate 2e<sup>-</sup>/4e<sup>-</sup> ORR control for H<sub>2</sub>O<sub>2</sub> production and Zn-air battery assemble, *Appl. Catal. B: Environ.* 285 (2021), 119788.
- [23] P. Xia, C. Wang, Q. He, Z. Ye, I. Sirés, MOF-derived single-atom catalysts: the next frontier in advanced oxidation for water treatment, *Chem. Eng. J.* 452 (2023), 139446.
- [24] F. Yu, M. Zhou, X. Yu, Cost-effective electro-Fenton using modified graphite felt that dramatically enhanced on H<sub>2</sub>O<sub>2</sub> electro-generation without external aeration, *Electrochim. Acta* 163 (2015) 182–189.
- [25] Q. Zhang, M. Zhou, G. Ren, Y. Li, Y. Li, X. Du, Highly efficient electro-synthesis of hydrogen peroxide on a superhydrophobic three-phase interface by natural air diffusion, *Nat. Commun.* 11 (2020) 1–11.
- [26] H. He, B. Jiang, J. Yuan, Y. Liu, X. Bi, S. Xin, Cost-effective electrogeneration of H<sub>2</sub>O<sub>2</sub> utilizing HNO<sub>3</sub> modified graphite/polytetrafluoroethylene cathode with exterior hydrophobic film, *J. Colloid Interf. Sci.* 533 (2019) 471–480.
- [27] Y. Tian, D. Deng, L. Xu, M. Li, H. Chen, Z. Wu, S. Zhang, Strategies for sustainable production of hydrogen peroxide via oxygen reduction reaction: from catalyst design to device setup, *Nano Micro Lett.* 15 (2023) 1–45.
- [28] Q. Yang, W. Xu, S. Gong, G. Zheng, Z. Tian, Y. Wen, L. Peng, L. Zhang, Z. Lu, L. Chen, Atomically dispersed Lewis acid sites boost 2-electron oxygen reduction activity of carbon-based catalysts, *Nat. Commun.* 11 (2020) 5478.
- [29] Y. Tian, M. Li, Z. Wu, Q. Sun, D. Yuan, B. Johannessen, L. Xu, Y. Wang, Y. Dou, H. Zhao, S. Zhang, Edge-hosted atomic Co-N<sub>4</sub> sites on hierarchical porous carbon for highly selective two-electron oxygen reduction reaction, *Angew. Chem. Int. Ed.* 61 (2022), 02213296.
- [30] G. Daniel, Y. Zhang, S. Lanzalaco, F. Brombin, T. Kosmala, G. Granozzi, A. Wang, E. Brillas, I. Sirés, C. Durante, Chitosan-derived nitrogen-doped carbon electrocatalyst for a sustainable upgrade of oxygen reduction to hydrogen peroxide in UV-assisted electro-Fenton water treatment, *ACS Sustain. Chem. Eng.* 8 (2020) 14425–14440.
- [31] Y. Huang, W. Zhou, L. Xie, J. Li, Y. He, S. Chen, X. Meng, J. Gao, Y. Qin, Edge and defect sites in porous activated coke enable highly efficient carbon-assisted water electrolysis for energy-saving hydrogen production, *Renew. Energ* 195 (2022) 283–292.
- [32] C. Dong, K.S. Lee, Y. Cho, S. Wang, X. Fan, F. Bai, J.H. Park, K. Zhang, Precise synthesis of single-atom Mo, W, Nb coordinated with oxygen functional groups of graphene oxide for stable and selective two-electron oxygen reduction in neutral media, *J. Mater. Chem. A* 10 (2022) 9488–9496.
- [33] M. Mazzucato, C. Durante, Insights on oxygen reduction reaction to H<sub>2</sub>O<sub>2</sub>: the role of functional groups and textural properties on the activity and selectivity of doped carbon electrocatalysts, *Curr. Opin. Electrochem.* 35 (2022), 101051.
- [34] O. Crowther, B. Meyer, M. Morgan, M. Salomon, Primary Li-air cell development, *J. Power Sources* 196 (2011) 1498–1502.
- [35] N. Singh, H. Kakiuchida, T. Sato, R. Hōnes, M. Yagihashi, C. Urata, A. Hozumi, Omniphobic metal surfaces with low contact angle hysteresis and tilt angles, *Langmuir* 34 (2018) 11405–11413.
- [36] X. Zhu, X. Yang, C. Lv, S. Guo, J. Li, Z. Zheng, H. Zhu, D. Yang, New approach to create TiO<sub>2</sub>(B)/carbon core/shell nanotubes: Ideal structure for enhanced lithium ion storage, *ACS Appl. Mater. Inter.* 8 (2016) 18815–18821.
- [37] X. Zhang, F. Xiao, Q. Feng, J. Zheng, C. Chen, H. Chen, W. Yang, Preparation of SiO<sub>2</sub> nanoparticles with adjustable size for fabrication of SiO<sub>2</sub>/PMHS ORMOSIL superhydrophobic surface on cellulose-based substrates, *Prog. Org. Coat.* 138 (2020), 105384.
- [38] H. Lin, Q. Hu, T. Liao, X. Zhang, W. Yang, S. Cai, Highly hydrophobic cotton fabrics modified by poly(methylhydrogen) siloxane and fluorinated olefin: Characterization and applications, *Polymers* 12 (2020) 833.
- [39] Z. Liu, X. Pang, K. Wang, X. Lv, X. Cui, Superhydrophobic coatings prepared by the in situ growth of silicone nanofilaments on alkali-activated geopolymers surface, *ACS Appl. Mater. Interf.* 11 (2019) 22809–22816.
- [40] Z. Liu, J. Yu, W. Lin, W. Yang, R. Li, H. Chen, X. Zhang, Facile method for the hydrophobic modification of filter paper for applications in water-oil separation, *Surf. Coat. Tech* 352 (2018) 313–319.
- [41] M. Wójcik-Bania, A. Łącz, A. Nyczyk-Malinowska, M. Hasik, Poly(methylhydroxysiloxane) networks of different structure and content of Si-H groups: Physicochemical properties and transformation into silicon oxycarbide ceramics, *Polymer* 130 (2017) 170–181.
- [42] A.V. Kuzmin, B.A. Shainyan, Single Si-doped graphene as a catalyst in oxygen reduction reactions: an in silico study, *ACS Omega* 5 (2022) 15268–15279.
- [43] V.M. Truong, N.B. Duong, H. Yang, Comparison of carbon supports in anion exchange membrane fuel cells, *Materials* 13 (2020) 5370.
- [44] G. Cihanoglu, Ö. Ebil, CVD-deposited oxygen-selective fluorinated siloxane copolymers as gas diffusion layers, *Ind. Eng. Chem. Res.* 61 (2022) 2633–2642.
- [45] Z. Qi, H. Dong, H. Yu, M. Zhao, H. Yu, In-situ electrochemical NO<sub>x</sub> removal process for the lean-burn engine exhaust based on carbon black gas diffusion electrode, *J. Clean. Prod.* 151 (2017) 465–474.
- [46] O. Garcia-Rodriguez, Y. Lee, H. Olvera-Vargas, F. Den, Z. Wang, O. Lefebvre, Mineralization of electronic wastewater by electro-Fenton with an enhanced graphene-based gas diffusion cathode, *Electrochim. Acta* 276 (2018) 12–20.
- [47] H. Zhang, Y. Li, Y. Zhao, G. Li, F. Zhang, Carbon black oxidized by air calcination for enhanced H<sub>2</sub>O<sub>2</sub> generation and effective organics degradation, *ACS Appl. Mater. Inter.* 11 (2019) 27846–27853.
- [48] T. Thami, L. Tauk, V. Flaud, Controlled structure and hydrophilic property of poly(methylhydroxysiloxane) thin films attached on silicon support and modified with phosphorylcholine group, *Thin Solid Films* 709 (2020), 138196.
- [49] Y. Wang, M. Wang, J. Wang, H. Wang, X. Men, Z. Zhang, A rapid, facile and practical fabrication of robust PDMS@ starch coatings for oil-water separation, *J. Taiwan Inst. Chem. E* 99 (2019) 215–223.
- [50] F. Cao, D. Kim, X. Li, C.X. Feng, Y. Song, Synthesis of polyaluminocarbosilane and reaction mechanism study, *J. Appl. Polym. Sci.* 85 (2002) 2787–2792.
- [51] P. Ding, L. Cui, D. Li, W. Jing, Innovative dual-compartment flow reactor coupled with a gas diffusion electrode for in situ generation of H<sub>2</sub>O<sub>2</sub>, *Ind. Eng. Chem. Res.* 58 (2019) 6925–6932.
- [52] Y. Zhu, F. Deng, S. Qiu, F. Ma, Y. Zheng, R. Lian, Enhanced electro-Fenton degradation of sulfonamides using the N, S co-doped cathode: Mechanism for H<sub>2</sub>O<sub>2</sub> formation and pollutants decay, *J. Hazard. Mater.* 403 (2021), 123950.
- [53] X. Yu, M. Zhou, G. Ren, L. Ma, A novel dual gas diffusion electrodes system for efficient hydrogen peroxide generation used in electro-Fenton, *Chem. Eng. J.* 263 (2015) 92–100.
- [54] W. Wang, Y. Li, Y. Li, M. Zhou, O.A. Arotiba, Electro-Fenton and photoelectro-Fenton degradation of sulfamethazine using an active gas diffusion electrode without aeration, *Chemosphere* 250 (2020), 126177.
- [55] B. Garza-Campos, D. Morales-Acosta, A. Hernández-Ramírez, J.L. Guzmán-Mar, L. Hinojosa-Reyes, J. Manríquez, E.J. Ruiz-Ruiz, Air diffusion electrodes based on synthesized mesoporous carbon for application in amoxicillin degradation by electro-Fenton and solar photo electro-Fenton, *Electrochim. Acta* 269 (2018) 232–240.
- [56] X. Sun, J. Lv, Z. Yan, Z. Sun, A three-dimensional gas diffusion electrode without external aeration for producing H<sub>2</sub>O<sub>2</sub> and eliminating amoxicillin using electro-Fenton, *Process, J. Environ. Chem. Eng.* 10 (2022), 107301.

- [57] Z. Zhang, H. Meng, Y. Wang, L. Shi, X. Wang, S. Chai, Fabrication of graphene@graphite-based gas diffusion electrode for improving H<sub>2</sub>O<sub>2</sub> generation in Electro-Fenton process, *Electrochim. Acta* 260 (2018) 112–120.
- [58] G.O. Santos, P.J.M. Cordeiro-Junior, I. Sánchez-Montes, R.S. Souto, M.S. Kronka, M.R. Lanza, Recent advances in H<sub>2</sub>O<sub>2</sub> electrosynthesis based on the application of gas diffusion electrodes: challenges and opportunities, *Curr. Opin. Electrochem.* 36 (2022), 101124.
- [59] Z. Ye, J.A. Padilla, E. Xuriguera, E. Brillas, I. Sirés, Magnetic MIL(Fe)-type MOF-derived N-doped nano-ZVI@C rods as heterogeneous catalyst for the electro-Fenton degradation of gemfibrozil in a complex aqueous matrix, *Appl. Catal. B: Environ.* 266 (2022), 118604.
- [60] Z. Xie, C. He, H. Zhou, L. Li, Y. Liu, Y. Du, W. Liu, Y. Mu, B. Lai, Effects of molecular structure on organic contaminants' degradation efficiency and dominant ROS in the advanced oxidation process with multiple ROS, *Environ. Sci. Technol.* 56 (2022) 8784–8795.
- [61] B.W. Zhang, T. Zheng, Y. Wang, Y. Du, S. Chu, Z. Xia, R. Amal, S. Dou, L. Dai, Highly efficient and selective electrocatalytic hydrogen peroxide production on Co-OC active centers on graphene oxide, *Commun. Chem.* 5 (2022) 1–7.